SUPPORTING INFORMATION

Morphological Dependent Exciton Dynamics and Thermal Transport in $MoSe_2$ Film

Jay Deep Gupta, Priyanka Jangra, Bishnu Pada Majee, and Ashish Kumar Mishra
School of Materials Science and Technology, Indian Institute of Technology (Banaras Hindu University), Varanasi-221005, India
Email: akmishra.mst@iitbhu.ac.in

S1. Schematic of CVD synthesis

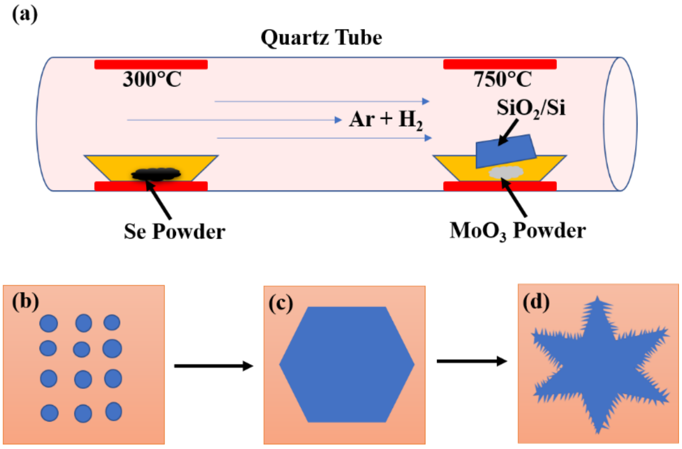

Fig. S1 Schematic diagram of (a) CVD setup to synthesize $MoSe_2$ and (b, c, d) the growth mechanism for hexagonal and snowlike $MoSe_2$.

S2. Raman mapping

The room temperature Raman mapping of $MoSe_2$ film clearly shows the presence of defect (D) peak throughout the region in snowlike $MoSe_2$, whereas it is missing in hexagonal $MoSe_2$.

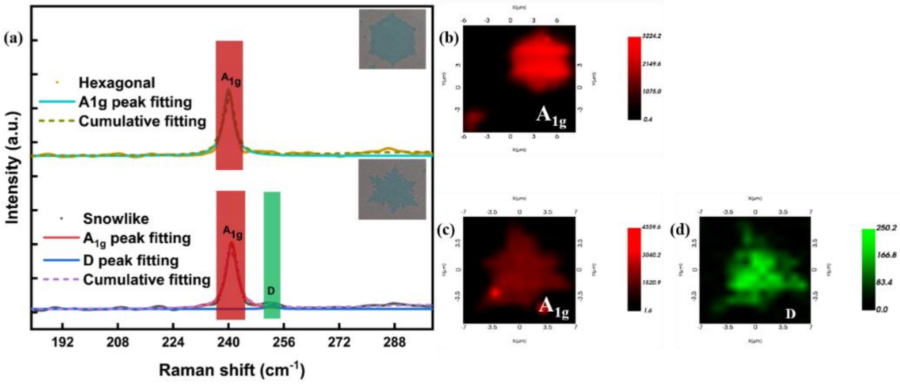

Fig. S2 (a) Raman spectra of hexagonal (up) and snowlike (down) $MoSe_2$ with Raman mapping images (b, c) corresponding to A_{1g} peak and (d) corresponding to defect (D) peak of $MoSe_2$.

S3. Density functional studies

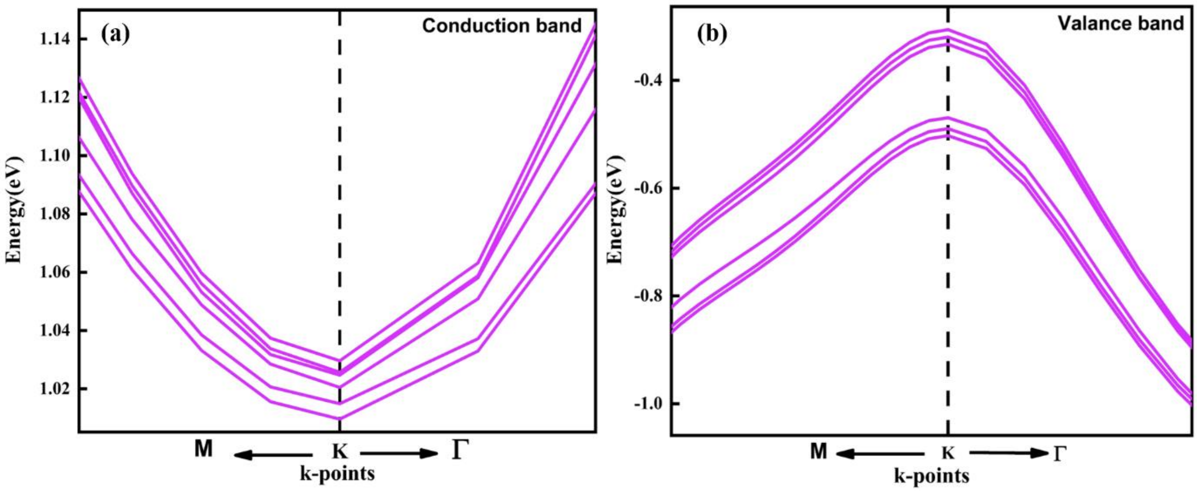

Fig. S3 Breaking of degeneracy in (a) conduction band and (b) valance band at K- point for 3L-$MoSe_2$ due to absence of inversion symmetry.

S4. Configurational coordinate diagram

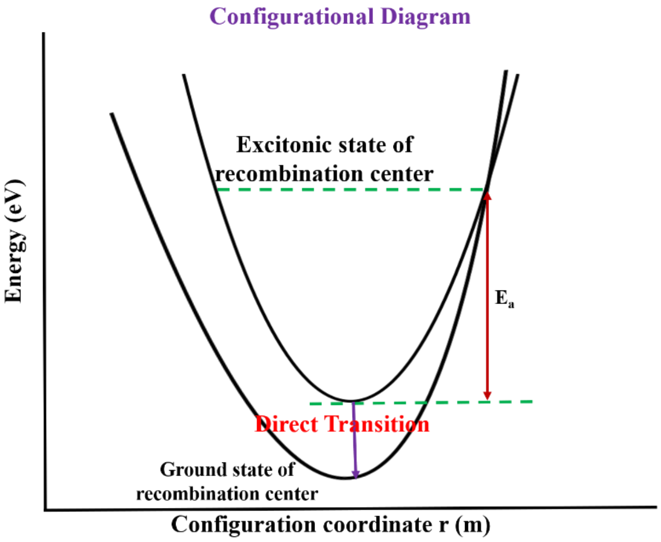

Fig. S4 Configurational diagram depicting Mott-Seitz mechanism in $MoSe_2$.

S5. FWHM of temperature-dependent PL

The variations of full width at half maximum (FWHM) for high energy exciton (E_H) of snowlike and hexagonal $MoSe_2$ film in the temperature range 93-300 K are shown in **Fig. S5**. Due to defect-related inhomogeneous broadening and enhanced phonon–exciton interaction, the FWHM for the A exciton increases linearly with increasing temperature. The lattice vibrations increase at higher temperatures, which enhances electron-phonon scattering.

Additionally, the nonradiation process causes an increase in FWHM and decrease in PL intensity.

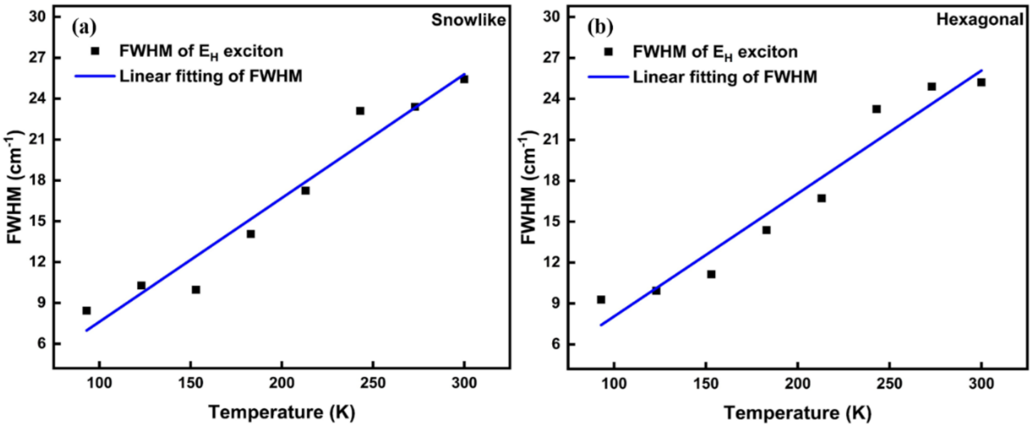

Fig. S5 Temperature dependence of FWHM for PL spectra of (a) snowlike (b) hexagonal $MoSe_2$ film over SiO_2/Si using LWD 50X objective lens.

S6. Temperature-dependent Raman

Temperature-dependent Raman spectra at remaining temperatures for prepared snowlike and hexagonal $MoSe_2$ film are shown in **Fig. S6**. The corresponding variation of FWHM for Raman modes are shown, indicating increase in FWHM with temperature.

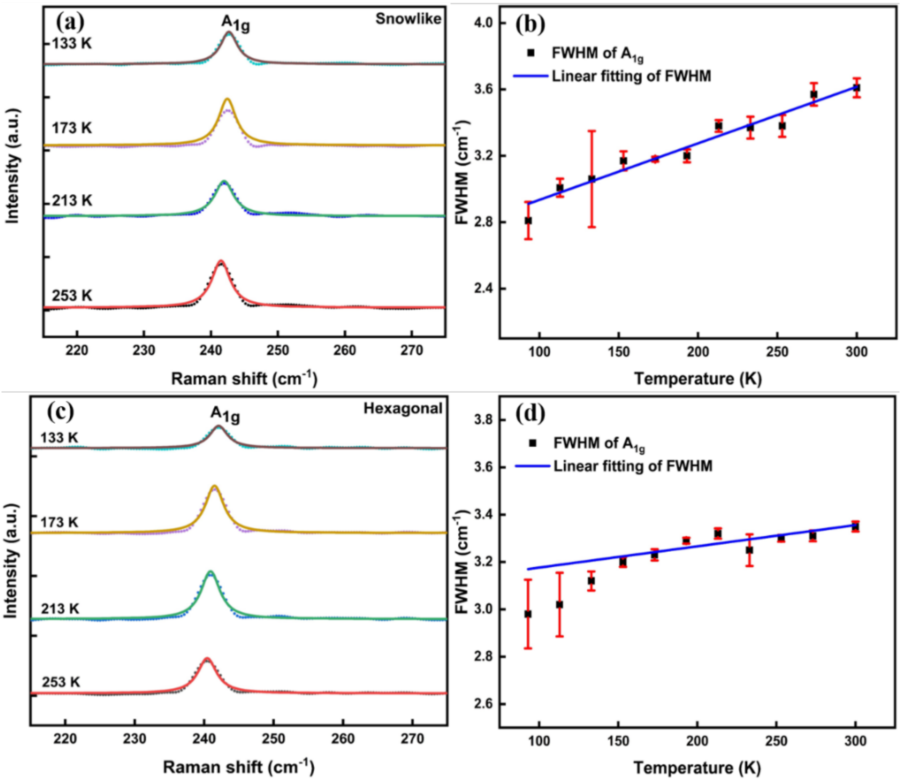

Fig. S6 Temperature-dependent Raman spectra for (a) snowlike and (c) hexagonal $MoSe_2$ film and (b, d) their corresponding FWHM, using LWD 50X objective lens.

S7. Power-dependent Raman

Power-dependent Raman spectra using 100X objective lens for prepared snowlike and hexagonal $MoSe_2$ film over SiO_2/Si substrate are shown in **Fig. S7**. In **Fig. S7**, we observe that the incident laser power causes an increase in the FWHM of the A_{1g} mode. The lattice expansion and bond softening are the primary reason for the observed redshift in Raman modes and rise in FWHM with laser intensity.

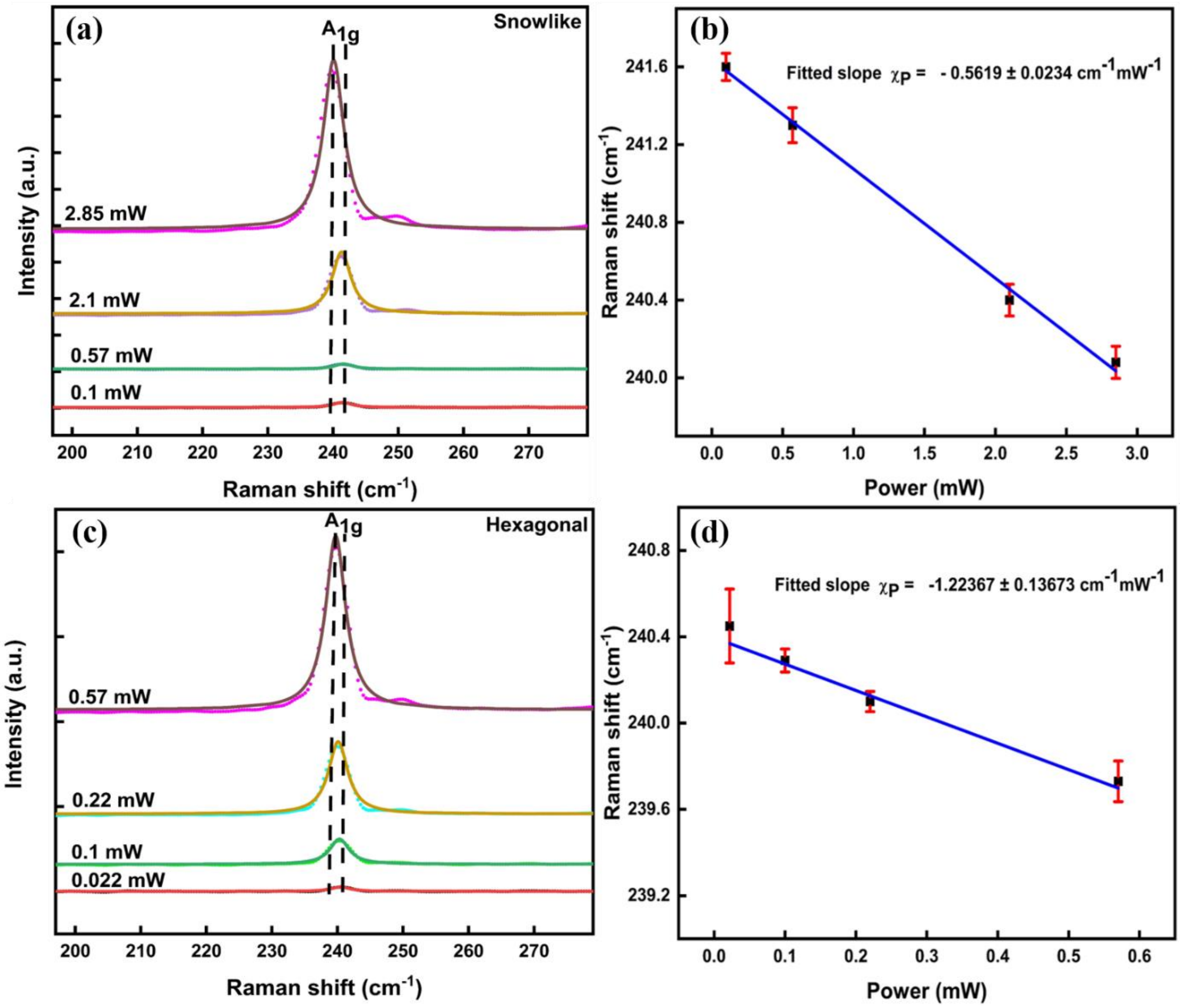

Fig. S7 Lorentzian fitted power-dependent Raman spectra for (a) snowlike and (c) hexagonal $MoSe_2$ and (b,d) their corresponding Raman shifts with incident laser power, using 100X objective lens.

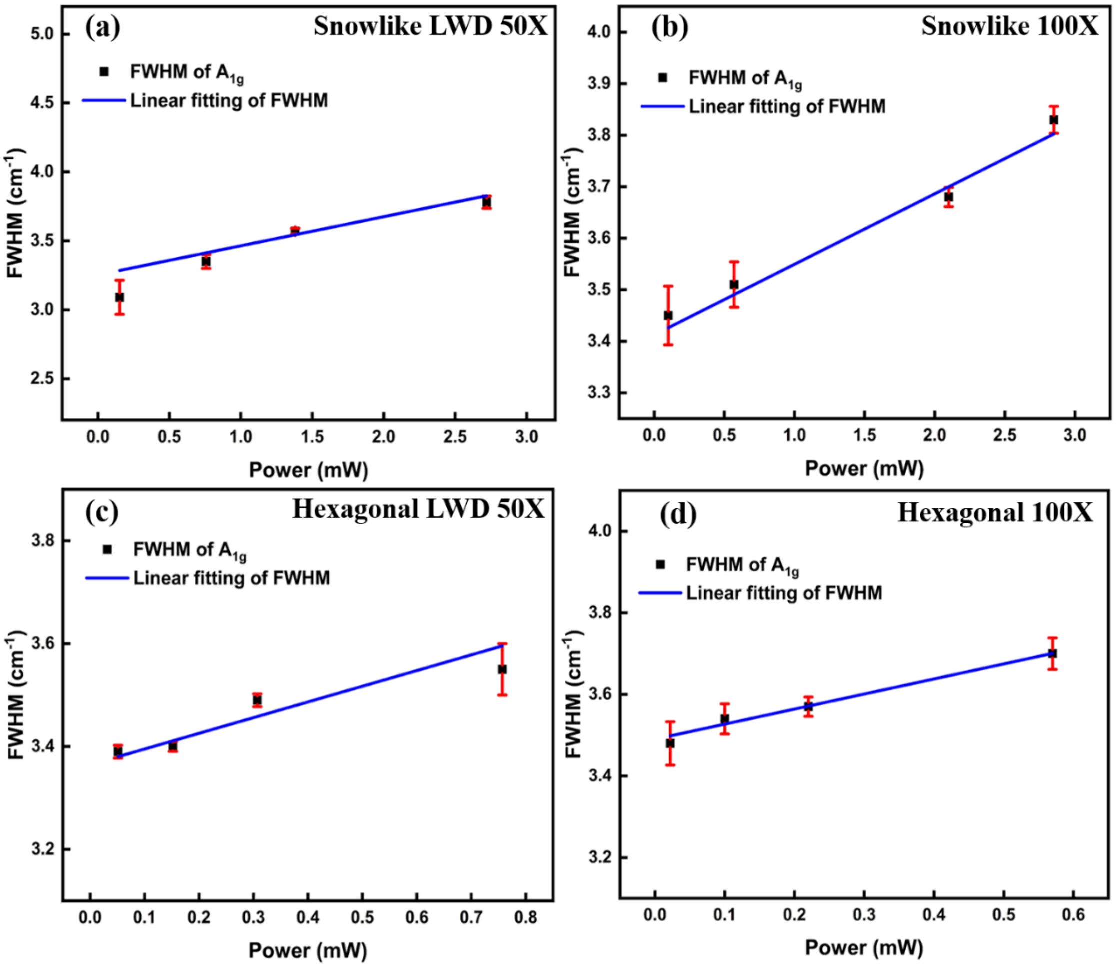

Fig. S8 Power dependence of FWHM using LWD 50X objective lens for (a) snowlike $MoSe_2$, and (c) hexagonal $MoSe_2$ film; power dependence of FWHM using 100X objective lens for (b) snowlike $MoSe_2$, and (d) hexagonal $MoSe_2$ film.

S8. Calculations of laser spot size at different objective lenses

The minimum laser spot size by the following formula can be given by[S1–S4]

$$r_0 = \frac{\lambda}{\pi \times N.A}\ nm \qquad (1)$$

Where, N.A is the numerical aperture of the objective lens and wavelength of the laser is denoted by λ.

For 100X objective lens (N.A.= 0.9), $r_0 = \frac{532}{3.14 \times 0.9} = 0.188 \sim 0.19\ \mu m$

Similarly, for LWD 50X (N.A.=0.6), $r_0 = 0.282 \sim 0.28\ \mu m$

Thus, the radius of the laser spot size for 100X and LWD 50X lenses are ~ 0.19×10^{-6} m and ~ 0.28×10^{-6} m, respectively.

S9. Calculation of α_a value for trilayer MoSe$_2$

For supported monolayer MoSe$_2$ we have chosen the value of absorption coefficient (α) 0.057 according to reported literature[S5] then we calculated the value of trilayer MoSe$_2$ absorption coefficient by using the following equation[S6]

$$\alpha_{a_{n+1}} = \alpha_{a_n} + (1 - \alpha_{a_n})\alpha_{a_{SL}} \tag{2}$$

α_{a_2} = 0.057 $+(1-0.057)0.057$ =0.111

α_{a_3} = 0.111 $+(1-0.111)0.057$ =0.161

S10. Calculations of R$_m$ values at different objective lenses:

(a) Snowlike shaped MoSe$_2$ film

χ_P= - 0.4797 cm^{-1}mW^{-1} for LWD 50X objective lens

χ_P= - 0.5619 cm^{-1}mW^{-1} for 100X objective lens

χ_T= - 0.0096 cm^{-1}K^{-1}

Therefore,

$R_{m1} = {}^{\chi_P}/_{\alpha\chi_T}$=3.2886×10^5 KW^{-1}

$R_{m2} = {}^{\chi_P}/_{\alpha\chi_T}$=3.8521×10^5 KW^{-1}

(b) Hexagonal shaped MoSe$_2$ film

χ_P= - 0.8307 cm^{-1}mW^{-1} for LWD 50X objective lens

χ_P= - 1.2236 cm^{-1}mW^{-1} for 100X objective lens

χ_T= -0.0115 cm^{-1}K^{-1}

Therefore,

$R_{m1} = {}^{\chi_P}/_{\alpha\chi_T}$=4.4871×10^5 KW^{-1}

$R_{m2} = {}^{\chi_P}/_{\alpha\chi_T}$=6.6086×10^5 KW^{-1}

References:

S1. W. Cai, A. L. Moore, Y. Zhu, X. Li, S. Chen, L. Shi and R. S. Ruoff, *Nano Letter*, 2010, **10**, 1645–1651.

S2. R. Yan, J. R. Simpson, S. Bertolazzi, J. Brivio, M. Watson, X. Wu, A. Kis, T. Luo, A. R. Hight Walker, H. G. Xing, *ACS Nano*, 2014**, 8**, 986–993.

S3. A. P. Gertych, A. Łapińska, K. Czerniak-Łosiewicz, A. Dużyńska, M. Zdrojek, J. Judek, *Scientific reports*, 2019, **9**, 1-7.

S4. B. P. Majee, J. D. Gupta, A. Sanskrityayn and A. K Mishra, *Journal of Physical Chemistry C*, 2021, **125**, 14865–14873.

S5. X. Zhang, D. Sun, Y. Li, G. H. Lee, X. Cui, D. Chenet, Y. You, T. F. Heinz and J. C. Hone, *ACS Applied Materials & Interfaces*, 2015, **7**, 25923–25929.

S6. J. Judek, A. P. Gertych, M. Winiarski, A. Lapińska, A. Duzuńska, M. Zdrojek, *Scientific reports*, 2015, **5**, 1-11.